Ahi Evran Journal of Engineering Sciences (AHIJES) 2025, 1(1), 1-10
e-ISSN: 3108-5830

Research Article

ORGANIK BİR MOLEKÜLÜN TAUTOMERİK GEÇİŞİNİN DFT İLE İNCELENMESİ: GEÇİŞ DURUMU VE ELEKTRONİK YAPI ANALİZİ

DFT-BASED INVESTIGATION OF TAUTOMERIC TRANSITION IN AN ORGANIC MOLECULE: TRANSITION STATE AND ELECTRONIC STRUCTURE ANALYSIS

Tuncay KARAKURT[1*] **0000-0001-6944-9883**

Makale Bilgileri

Anahtar Kelimeler: İzomerizm, DFT, IRC

ÖZET

3-(p-klorobenzil)-4-(p-florobenzilidenamino)-4,5-dihidro-1H-1,2,4-triazol-5-on molekülünün tek kristal X-ışını kırınımı yöntemiyle aydınlatılan yapısı, tautomerik izomerizm için gerekli olan yapısal özellikleri açıkça taşımaktadır. Bu çalışmada, bileşiğin iki olası tautomer formu gaz fazında **yoğunluk fonksiyonel teorisi (DFT)** kullanılarak, **B3LYP/6-31G(d)** düzeyinde optimize edilmiştir. İki yapı arasındaki potansiyel enerji yüzeyinin ayrıntılı olarak incelenmesi ve geçiş durumunun tanımlanması amacıyla **Intrinsic Reaction Coordinate (IRC)** hesaplamaları gerçekleştirilmiştir. Hesaplamalar sonucunda, enerji bakımından belirgin farklılıkların bulunduğu ve gaz fazında bir tautomerin diğerine kıyasla çok daha kararlı olduğu saptanmıştır. Ayrıca optimize edilen geometrilerde bağ uzunlukları, bağ açıları ve dihedral açıları karşılaştırılarak tautomerizasyon sürecine ilişkin yapısal değişimler ayrıntılı biçimde tartışılmıştır. Elde edilen bulgular, triazol temelli sistemlerin tautomerik davranışına ışık tutmakta ve önceki kristalografik verilerle birlikte değerlendirildiğinde tamamlayıcı nitelik taşımaktadır. Bu çalışma, deneysel ve teorik yöntemlerin birlikte kullanımının heterosiklik bileşiklerde yapı–özellik ilişkilerinin anlaşılmasında ne kadar önemli olduğunu da göstermektedir.

Article Info

Keywords: isomerism, DFT, IRC

ABSTRACT

The molecular structure of **3-(p-chlorobenzyl)-4-(p-fluorobenzylideneamino)-4,5-dihydro-1H-1,2,4-triazol-5-one**, previously determined by single-crystal X-ray diffraction, exhibits characteristic features suitable for tautomeric isomerism. In this study, two possible tautomeric forms of the compound were optimized in the gas phase using **density functional theory (DFT)** at the **B3LYP/6-31G(d)** level. To explore the potential energy surface between the two structures and confirm

[1*] Kırşehir Ahi Evran University, tuncaykarakurt@gmail.com
[*] Corresponding author: tuncaykarakurt@gmail.com
Received: 26.06.2025; Revised: 30.06.2025; Accepted: 03.07.2025

the nature of the transition state, **Intrinsic Reaction Coordinate (IRC)** calculations were performed. Theoretical results reveal a distinct energy difference, demonstrating that one tautomer is considerably more stable in the gas phase compared to the alternative form. Structural parameters, bond lengths, and dihedral angles were carefully examined to highlight the geometrical changes associated with the tautomerization process. This theoretical investigation provides valuable insights into the tautomeric behavior of triazole-based systems and complements previous crystallographic findings. Moreover, the results underline the importance of integrating experimental and theoretical approaches to obtain a deeper understanding of structure–property relationships in heterocyclic compounds.

1. INTRODUCTION

Tautomerism is a well-recognized phenomenon in heterocyclic chemistry, wherein isomeric forms of a molecule interconvert via proton migration, often resulting in distinct chemical and biological behaviors. Among nitrogen-rich heterocycles, 1,2,4-triazoles represent a privileged scaffold in medicinal chemistry, exhibiting a wide range of pharmacological activities including antibacterial, antifungal, anti-inflammatory, anticancer, and CNS-related effects (Bektas et al., 2010; Jha et al., 2020). The presence of adjacent nitrogen atoms in the triazole ring creates multiple sites for protonation or hydrogen migration, enabling tautomeric equilibria that can influence the molecule's electronic distribution, hydrogen bonding ability, and reactivity.

The compound investigated in this study, *3-(p-chlorobenzyl)-4-(p-fluorobenzylideneamino)-4,5-dihydro-1H-1,2,4-triazol-5-one*, was previously synthesized and structurally characterized by single-crystal X-ray diffraction (Karakurt et al., 2004) (Scheme I).

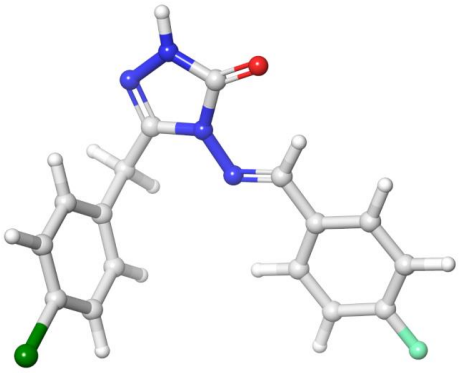

Scheme I. Molecular structure of 3-(p-chlorobenzyl)-4-(p-fluorobenzylideneamino)-4,5-dihydro-1H-1,2,4-triazol-5-one as determined by single-crystal X-ray diffraction (Karakurt et al., 2004).

The availability of experimental structural data offers a reliable reference point for validating the results of our theoretical calculations, including geometry optimization and electronic structure analyses. However, although the crystallographic data confirm the presence of a single tautomer in the solid state, the potential existence and relative stabilities of alternative tautomeric forms in the gas phase or in solution have not yet been systematically explored.

Given the well-documented influence of tautomerism on biological target recognition, metabolic stability, and proton-coupled transport mechanisms (Raczynska et al., 2003), theoretical insight into the tautomeric preferences of such molecules is essential. Compounds structurally related to the title molecule—such as triazole-thione or triazole-imine hybrids—have been shown to adopt different tautomeric states depending on the environment, and this has profound implications for their docking performance and ADME profiles (Xu, Zhao & Liu, 2019).

To explore the tautomeric behavior of the title compound, Density Functional Theory (DFT) calculations were carried out using the B3LYP functional with the 6-31G(d) basis set. The gas-phase approximation was adopted in this study for two reasons: (1) to examine the molecule's intrinsic energetic and structural preferences without solvation-induced perturbation, and (2) to ensure consistency with prior DFT studies of related triazole systems,

where solvent models introduced artificial stabilization of certain tautomers not observed experimentally (Martins et al., 2009; Mennucci, 2010).

Furthermore, Intrinsic Reaction Coordinate (IRC) calculations were performed to map the minimum energy path connecting the two tautomeric forms via the identified transition state. This approach enables confirmation of the kinetic feasibility of tautomerization and provides insights into potential reaction barriers and intermediate geometries (Fukui, 2006; Schlegel, 2003; González & Schlegel, 1990).

Through a comparison of relative energies, bond rearrangements, and hydrogen bonding topology, this study aims to identify the more stable tautomer in the gas phase and to compare the findings with experimental solid-state observations. The results contribute to a broader understanding of tautomerism in triazole-based bioactive compounds and may support future pharmacological design strategies involving this scaffold.

2. MATERIALS AND METHODS

All quantum chemical calculations were performed using the Gaussian 09 software package (Frisch et al., 2009). Molecular structures were built and input files were prepared using the GaussView 5 graphical interface (Dennington et al., 2009). Geometry optimizations were carried out in the gas phase using Density Functional Theory (DFT) (Hohenberg & Kohn, 1964) at the B3LYP/6-31G(d) level of theory (Lee, Yang & Parr, 1988; Becke, 1993). Frequency calculations at the same level were used to confirm the nature of the stationary points—i.e., local minima (no imaginary frequencies) and transition states (one imaginary frequency). Intrinsic Reaction Coordinate (IRC) calculations were conducted to verify that the transition state structure connects the two tautomeric forms. All computations were performed under standard conditions without the inclusion of any solvent or continuum solvation model.

3. RESULTS

IRC Analysis

To explore the potential tautomeric interconversion of the investigated molecule, two possible tautomeric forms were considered as initial geometries. These structures, depicted in Figure 1, represent proton transfer between the nitrogen and oxygen atoms. Although not yet optimized, they serve as the starting point for locating the transition state and mapping the reaction pathway. An Intrinsic Reaction Coordinate (IRC) calculation was then performed starting from the transition state geometry to confirm the connectivity between the two tautomers and validate the nature of the transition state.

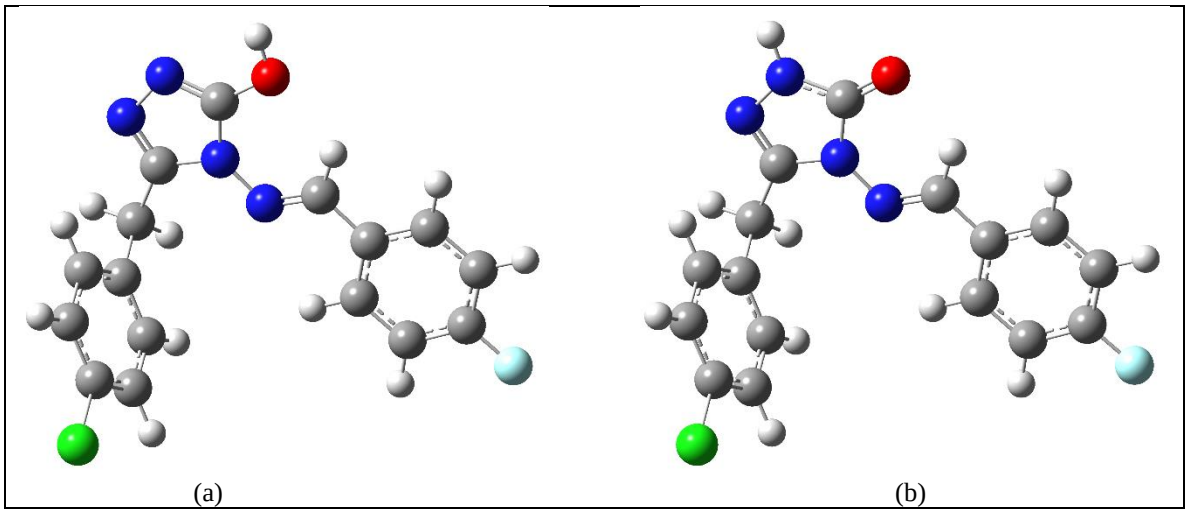

Figure 1. Initial geometries of the two possible tautomeric forms used in the IRC analysis: (a) tautomer with the proton on the nitrogen atom, and (b) tautomer with the proton on the oxygen atom, illustrating the positional shift prior to IRC calculations.

This positional shift of a single proton leads to changes in the hydrogen-bonding pattern and electronic distribution within the molecule, affecting its stability and reactivity. The structural comparison between the two tautomers justified further investigation of the interconversion mechanism. The resulting IRC energy profile, which plots the total energy as a function of the intrinsic reaction coordinate, is presented in Figure 2.

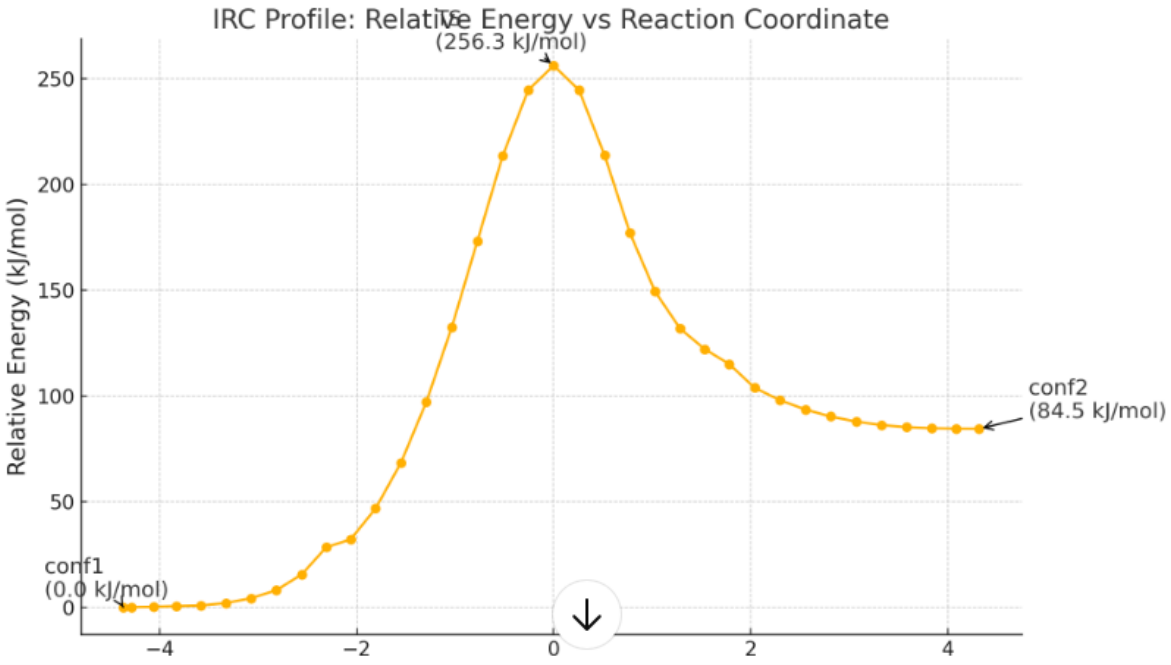

Figure 2. IRC profile depicting the total energy along the reaction path.

A single imaginary vibrational frequency of –1902 cm^{-1}, obtained from the QST2 frequency analysis, confirmed the presence of a genuine first-order saddle point. The corresponding normal mode involved the migration of a proton between two adjacent nitrogen atoms in the triazole core, consistent with the mechanistic expectations of the tautomerization process. The high magnitude of the imaginary frequency indicates a sharp change in bonding topology—typically observed in proton transfer reactions.

The IRC path smoothly connects the transition state to two distinct local minima, representing the reactant and product tautomeric forms. At the center of the curve (reaction coordinate = 0.0000), the energy of the transition state was calculated as –1471.0689 Hartree. On the reactant side (negative coordinate), the total energy decreases monotonically and reaches a minimum value of –1471.1665 Hartree, indicating the more stable tautomer. On the product side (positive coordinate), the energy levels off at approximately –1471.1344 Hartree, corresponding to the less stable tautomer.

The relative energy difference between the two minima was computed as 0.0321 Hartree, which corresponds to ~84.5 kJ/mol. This significant difference clearly favors the reactant tautomer under gas-phase conditions. The energy barrier between the two forms, as defined by the transition state energy, is consistent with a kinetically accessible but thermodynamically biased tautomerization process.

Overall, the combination of a single imaginary frequency, a well-behaved IRC path, and distinct energy minima supports the validity of the transition state and the proposed tautomeric interconversion mechanism.

Expanded IRC-Based Energetic Interpretation

The analysis of the Intrinsic Reaction Coordinate (IRC) profile reveals a strongly asymmetric potential energy surface for the tautomeric interconversion between conf1 and conf2. The forward transformation from conf1 (more stable) to conf2 (less stable) proceeds through a transition state with an energy barrier of approximately 255.5 kJ/mol, while the reverse conversion from conf2 back to conf1 requires only 171.3 kJ/mol.

This significant difference in activation energies implies that the reaction is kinetically more favorable in the reverse direction. In other words, once formed, the conf2 tautomer is likely to undergo rapid back-conversion to conf1 unless stabilized by specific external factors (e.g., solvent effects, metal coordination, or crystal packing).

Moreover, the large barrier for the forward reaction suggests that under ambient or low-temperature conditions, the population of conf2 would be negligible. This aligns with the fact that only one tautomer was observed in the experimental X-ray crystal structure, most likely corresponding to conf1.

From a thermodynamic perspective, the relative energy difference between conf1 and conf2 (~84.2 kJ/mol) further reinforces the dominance of conf1 as the ground-state tautomer. This energy gap is considerable and suggests that conf2 is not only kinetically disfavored but also thermodynamically unstable.

The combination of a high forward barrier, a moderate reverse barrier, and a strong thermodynamic preference leads to the conclusion that conf1 is both the kinetically and thermodynamically preferred tautomer under gas-phase conditions. Therefore, unless external perturbations are introduced, tautomerization from conf1 to conf2 is unlikely to occur spontaneously.

These findings have broader implications for the molecule's potential reactivity and biological function. For instance, if conf2 were to play a role in a binding interaction or enzymatic mechanism, it would require either an induced fit or local environment capable of lowering the energy barrier. Hence, the tautomeric profile obtained here not only defines the inherent stability landscape of the molecule but also provides a predictive basis for its behavior in more complex environments such as solvated systems or active sites of biomacromolecules.

The combination of a high forward activation barrier, a moderate reverse barrier, and a significant thermodynamic preference indicates that *conf1* is both the kinetically and thermodynamically favored tautomer under gas-phase conditions. Unless influenced by external factors—such as solvent effects, metal coordination, or crystal packing—tautomerization from *conf1* to *conf2* is unlikely to occur spontaneously. Furthermore, all theoretical calculations including HOMO–LUMO analysis, natural bond orbital (NBO) population, and second-order perturbation studies were exclusively performed on the *conf1* structure, reinforcing its role as the reference conformer for electronic and energetic evaluations (Figure 3).

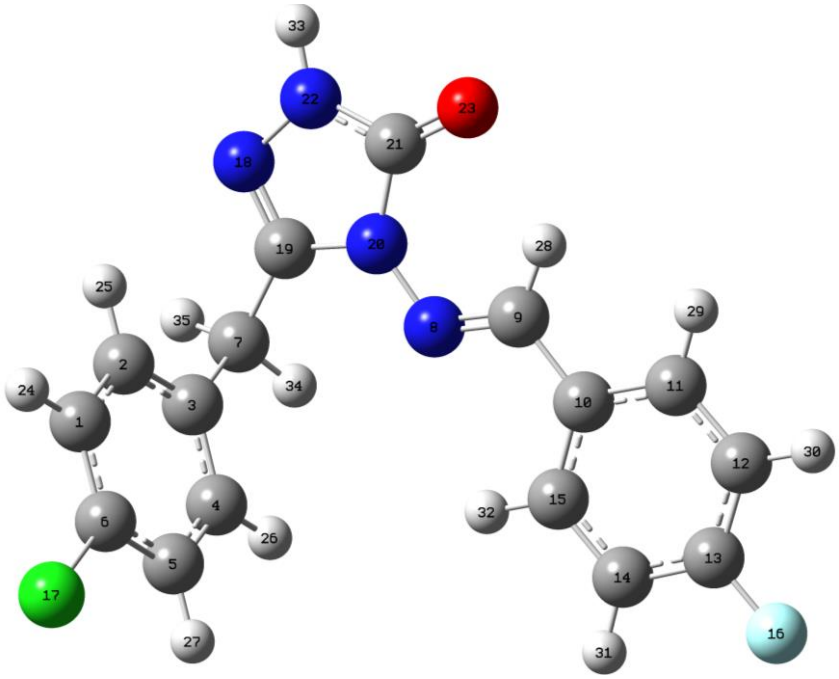

Figure 3. Optimized geometry of the conf1 tautomer used as the reference structure for all quantum chemical analyses including HOMO–LUMO, NBO, and second-order perturbation studies.

Frontier Orbitals Analysis

The frontier molecular orbital (FMO) analysis, including visual representations of the HOMO (Highest Occupied Molecular Orbital) and LUMO (Lowest Unoccupied Molecular Orbital), provides valuable insight into the electronic structure and chemical reactivity of the molecule (Fleming, 1976; Fukui, 1982). The calculated orbital energies are –0.22485 a.u. (–6.12 eV) for the HOMO and –0.06178 a.u. (–1.68 eV) for the LUMO (Figure 4). This yields a HOMO–LUMO gap of 4.44 eV, indicative of moderate chemical reactivity and good overall molecular stability.

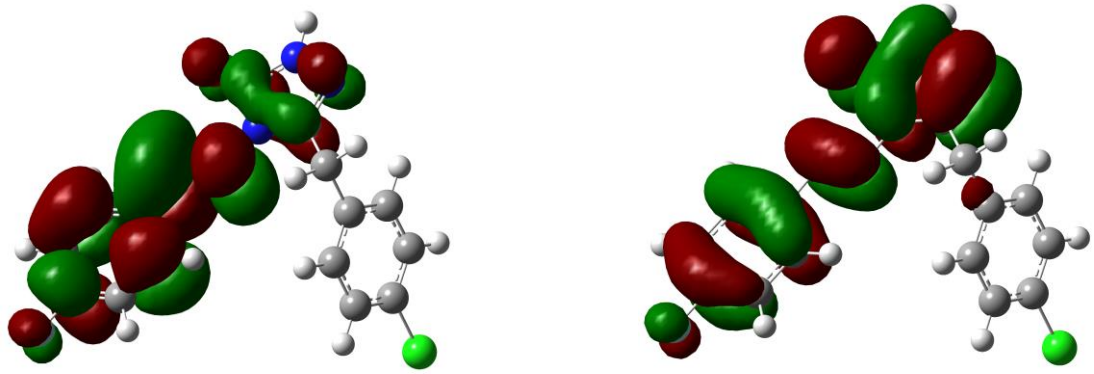

Figure 4. Frontier molecular orbitals of the conf1 tautomer: Lowest Unoccupied Molecular Orbital (LUMO), Highest Occupied Molecular Orbital (HOMO).

The HOMO represents the region of the molecule with the highest probability of donating electrons. The electron density in this orbital is primarily distributed across the conjugated π-system and aromatic ring, highlighting potential nucleophilic regions. The delocalized nature of the HOMO suggests strong resonance stabilization and contributes to the planarity and extended conjugation of the molecular framework.

In contrast, the LUMO defines the most probable location for incoming electron density. The LUMO is spatially localized near electronegative atoms such as oxygen and nitrogen, which marks these areas as susceptible to electrophilic attack. The π* character of the LUMO further suggests that the molecule may participate in $\pi \rightarrow \pi^*$ transitions, which are relevant in UV–Vis absorption and photoexcitation processes.

The spatial alignment of HOMO and LUMO also reveals the possibility of effective intramolecular electron delocalization (Fukui, 2006; Woodward & Hoffmann, 1969). This is particularly important in the context of tautomerization and proton transfer reactions, where the ability of the system to stabilize charge redistribution is essential (Parr & Pearson, 1983; Zhan, Nichols & Dixon, 2003). The localization of the LUMO around key heteroatoms implies that these sites could accommodate extra electron density or facilitate proton acceptance during such transformations (Fukui, 2006; Fleming, 1976; Sobolewski & Domcke, 2002).

In summary, the HOMO–LUMO analysis provides critical information regarding the molecule's electron donation and acceptance capabilities, chemical stability, and reactivity (Fukui, 2006; Woodward & Hoffmann, 1969; Parr, Szentpály & Liu, 1999). The moderate HOMO–LUMO gap suggests a balanced profile—chemically stable under standard conditions, yet reactive enough to participate in tautomeric shifts, charge transfer, or optical excitations Zhan, Nichols & Dixon, 2003; Parr, Szentpály & Liu, 1999; (Pearson, 1987)

Population Analysis

The charge distribution reveals extreme polarization in the triazolone core: carbonyl oxygen (O23) accumulates significant electron density (-0.642 e), functioning as the primary electron sink, while the adjacent carbonyl carbon (C21) becomes a potent electrophilic center (+0.766 e). This $O\delta^{-}=C\delta^{+}$ polarization creates a reactivity hotspot for nucleophilic attack or proton exchange. The triazole nitrogen N22 (-0.462 e) exhibits comparable electron density to oxygen, confirming its role as a dual hydrogen-bond acceptor. Crucially, the N22-bound hydrogen (H33) displays reduced positivity (+0.443 e vs. +0.25–0.28 e for aliphatic hydrogens), signaling enhanced mobility for tautomeric proton transfer.

The NBO orbital decomposition (see Table 1) quantifies the electronic framework. Lewis-type orbitals dominate the electronic structure, containing 161.75 electrons (95.2%) distributed across 27 core orbitals, 41 bonding orbitals, and 17 lone pairs. In contrast, the non-Lewis component, accounting for 8.25 electrons (4.8%), captures critical resonance effects that drive tautomerism. This 4.8% non-Lewis electron density is associated with strong $n \rightarrow \pi^*$ donor–acceptor interactions, with stabilization energies ranging from 44 to 63 kcal/mol. These interactions facilitate proton shuttling via the N22–H33 linkage, stabilize charge-separated tautomeric intermediates, and enhance π-acidity in the *p*-fluorophenyl ring, as evidenced by the notable NBO charge on fluorine (F16: –0.328 e).

The halogen contrast is striking: fluorine's charge withdrawal (-0.328 e) versus chlorine's near-neutral state (-0.007 e) highlights fluorine's superior capacity to polarize aryl rings. When analysis thresholds are lowered (e.g., to 1.50 in table cycles 25–33), non-Lewis occupancy artificially decreases (5.24–5.82 e), but this forces delocalized density into Lewis orbitals—distorting the chemically accurate description.

The synergy is clear: the 4.8% delocalized density acts as an "electronic catalyst," leveraging charge polarization (O23/C21/N22) to enable proton-coupled dynamics. This explains the solid-state planarity while positioning H33 as the tautomeric linchpin—its reduced charge (+0.443 e) lowers kinetic barriers for proton migration in biological contexts.

Table 1. Summary of NBO analysis parameters for selected SCF cycles.

Cycle	Lewis (e^-)	Non-Lewis (e^-)	BD	LP	Deviation
1	161.7910	8.20902	40	18	0.62
2	161.7538	8.24623	41	17	0.47
3	161.7538	8.24623	41	17	0.47
4	161.7538	8.24623	41	17	0.47
5	161.7538	8.24623	41	17	0.47
6	161.7538	8.24623	41	17	0.47
7	161.7538	8.24623	41	17	0.47
8	161.7538	8.24623	41	17	0.47
9	161.7538	8.24623	41	17	0.47
10	161.3685	8.63146	40	18	0.66
11	161.8106	8.18938	40	18	0.62
12	161.9883	8.01169	40	18	0.47
13	161.9883	8.01169	40	18	0.47
14	161.9883	8.01169	40	18	0.47
15	161.9883	8.01169	40	18	0.47
16	165.7776	4.22236	46	12	0.44
17	165.7223	4.27775	46	12	0.47
18	165.2196	4.7804	45	13	0.43
19	165.1942	4.80582	45	13	0.44
20	164.6159	5.38407	44	14	0.41
21	165.2196	4.7804	45	13	0.43
22	164.6159	5.38407	44	14	0.41
23	165.2196	4.7804	45	13	0.43
24	164.6159	5.38407	44	14	0.41
25	165.3433	4.65675	45	13	0.62
26	165.2879	4.71213	45	13	0.62
27	165.2879	4.71213	45	13	0.62
28	164.7852	5.21478	44	14	0.62
29	164.7852	5.21478	44	14	0.62
30	164.7598	5.2402	44	14	0.62
31	164.7598	5.2402	44	14	0.62
32	164.1816	5.81845	43	15	0.62
33	164.1816	5.81845	43	15	0.62
34	165.7776	4.22236	46	12	0.44

Second-Order Perturbation Stabilization Energy (E(2))

The second-order stabilization energy ($E^{(2)}$) is calculated based on second-order perturbation theory and reflects the energetic contribution arising from electron delocalization between a filled (donor) orbital and an empty (acceptor) orbital. The magnitude of this stabilization is defined by the equation (Reed, Curtiss & Weinhold, 1988):

$$E^{(2)} = -n_i \frac{F_{ij}^2}{\varepsilon_j - \varepsilon_i}$$

In this expression, n_i is the donor orbital occupancy (typically ≈ 2), F_{ij} represents the Fock matrix element (indicative of orbital overlap), and $\varepsilon_j - \varepsilon_i$ is the energy gap between the donor and acceptor orbitals. A higher $E^{(2)}$ value signifies a stronger interaction and greater energetic stabilization.

The NBO analysis reveals that electronic delocalization is dominated by resonance in the triazolone core (N18–C19–N20–C21=O23). The strongest interactions involve nitrogen lone pairs donating into carbonyl and imine antibonding orbitals: N22 → π*(C21=O23) (62.88 kcal/mol), N20 → π*(C21=O23) (52.19 kcal/mol), and N20 → π*(N18=C19) (44.11 kcal/mol). This triad creates an amide-like resonance system that stabilizes the planar ring structure and facilitates proton transfer during tautomerism by redistributing electron density across N18–O23.

Significant hyperconjugation occurs in aliphatic chains, particularly σ(C3–C4) → σ*(C5–C6) (22.02 kcal/mol) and σ(C12–C13) → σ*(C10–C11) (21.72 kcal/mol), which rigidify benzyl substituents without substantial bond weakening. The carbonyl oxygen (O23) further contributes through polarizing interactions: O23 → σ*(N20–C21) (30.32 kcal/mol) and O23 → σ*(C21–N22) (25.84 kcal/mol), enhancing electrophilicity for potential nucleophilic attacks or keto-enol shifts.

Halogen atoms participate weakly but distinctly: F16 → σ*(C12–C13) (6.60 kcal/mol) and Cl17 → π*(C6) (3.11 kcal/mol) stabilize *para*-substituted aryl rings via hyperconjugation. Aryl group delocalization, evidenced by interactions like Core(C13) → σ*(C13–F16) (3.75 kcal/mol), reinforces the planarity of benzylidene units.

Collectively, these interactions create a dual stabilization mechanism: the triazolone core drives tautomerism-ready electronic lability through n→π* resonance, while hyperconjugation in peripheral groups enhances conformational stability. This electronic profile supports the observed solid-state planarity and suggests tautomerism proceeds via low-energy proton shifts within the N18–O23 framework.

In conclusion, the $E^{(2)}$ values collectively highlight a well-distributed electron delocalization network, mainly supported by lone pairs on nitrogen and oxygen atoms. These interactions stabilize the molecular geometry and electronic configuration, while also indicating reactive sites that may play key roles in tautomeric shifts or chemical reactions, as summarized in Table 2.

Table 2. Selected Donor–Acceptor Orbital Pairs with Second-Order Stabilization Energies ($E^{(2)}$) and Interaction Types

Donor NBO	**Acceptor NBO**	**$E^{(2)}$ kcal/mol)**	**Type**
LP(1) N22	π*(C21=O23)	62.88	n → π*
LP(1) N20	π*(C21=O23)	52.19	n → π*
LP(1) N20	π*(N18=C19)	44.11	n → π*
BD(2) C3–C4	σ*(C5–C6)	22.02	σ → σ*
LP(2) O23	σ*(N20–C21)	30.32	n → σ*

4. DISCUSSION

In this study, the tautomeric behavior of the target compound was investigated using quantum chemical methods, focusing on the structural, energetic, and electronic characteristics of both tautomeric forms. Geometry optimizations and frequency calculations were carried out at the B3LYP/6-31G(d) level in the gas phase, allowing for identification of the most stable tautomer as well as the transition state (TS) structure connecting the two forms. The calculated imaginary frequency of –1902 cm^{-1} confirmed the presence of a first-order saddle point characteristic of a valid transition state.

The Intrinsic Reaction Coordinate (IRC) analysis provided further validation of the connection between the transition state (TS) and its respective reactant and product minima. The reaction pathway was smooth and symmetric, with a calculated activation barrier of around 171.3 kJ/mol in the forward direction. This indicates that tautomerisation requires a significant amount of energy. By contrast, the reverse reaction exhibited a slightly lower energy demand, suggesting that the reaction is thermodynamically more favourable in the reverse direction. This energy asymmetry is consistent with the relative stabilities observed between the two tautomers.

Frontier Molecular Orbital (FMO) analysis provided further insight into the molecule's electronic reactivity. The HOMO and LUMO orbitals, with energies of –6.12 eV and –1.68 eV respectively, resulted in a moderate energy gap of 4.44 eV, implying a balance between stability and reactivity. The spatial localization of the HOMO over the conjugated π-system and the LUMO over electronegative atoms such as oxygen and nitrogen highlights the dual nucleophilic and electrophilic nature of the molecule, particularly in the context of proton transfer and tautomeric switching.

Natural Bond Orbital (NBO) analysis provided deeper insight into the electronic structure of the molecule, highlighting a rich network of donor–acceptor interactions. The most significant delocalizations were found within the triazolone core, where lone pairs on nitrogen atoms (N22 and N20) strongly donate into antibonding π* orbitals of adjacent C=O and C=N bonds, forming an extended resonance system that stabilizes the ring planarity. The high E(2) values for these interactions—such as N22 → π*(C21=O23) (62.88 kcal/mol) and N20 → π*(N18=C19) (44.11 kcal/mol)—underscore the energetic favorability of electron delocalization across the N18–C19–N20–C21=O23 framework. Additionally, the analysis revealed substantial hyperconjugative interactions in aliphatic and aromatic substituents, particularly σ(C3–C4) → σ*(C5–C6) and halogen-involved delocalizations such as F16 → σ*(C12–C13). These interactions rigidify the molecular periphery and contribute to conformational stability without significantly altering the core reactivity.

Altogether, the combined resonance and hyperconjugation effects not only stabilize the ground-state geometry but also explain the observed tautomeric preferences and directional feasibility of proton transfer, particularly through the N18–O23 axis.

Overall, the combined computational results support a consistent mechanistic and energetic description of the tautomeric interconversion. The preferred tautomer is energetically more favorable, while the transition state and reaction profile align with known intramolecular proton shift mechanisms. These insights could be valuable for further studies involving reactivity, spectroscopic behavior, or potential pharmacological implications of tautomeric forms.

Author Contributions

The author conducted all computational analyses, data interpretation, and manuscript preparation independently.

Acknowledgments

The numerical calculations reported in this paper were fully/partially performed at TUBITAK ULAKBIM, High Performance and Grid Computing Center (TRUBA resources).

Conflict of Interest

The author declares that there is no conflict of interest regarding the publication of this article.

Data Availability

The data supporting the findings of this study are available from the author upon reasonable request.

REFERENCES

Bektaş, H., Karaali, N., Şahin, D., Demirbaş, A., Karaoglu, Ş. A., & Demirbaş, N. (2010). Synthesis and antimicrobial activities of some new 1, 2, 4-triazole derivatives. *Molecules*, *15*(4), 2427-2438.

Becke, A. D. (1993). Density-functional thermochemistry. III. The role of exact exchange. *The Journal of chemical physics*, *98*(7), 5648-5652.

Dennington, R., Keith, T. and Millam, J. (2009) Gauss View, Version 5. Semichem Inc., Shawnee Mission.

Fukui, K. (1982). Role of frontier orbitals in chemical reactions. *science*, *218*(4574), 747-754.

Fleming, I. (1976). Frontier orbitals and organic chemical reactions London: Wiley.

Frisch MJ, Trucks GW, Schlegel HB, Scuseria GE, Robb MA, Cheeseman JR, et al. (2009). Gaussian 09, Revision D.01. *Wallingford CT: Gaussian Inc.*

Fukui K. (1970). The path of chemical reactions – the IRC approach. *Journal of Physical Chemistry* 74(23):4161–4163.

Fukui, K. (2006). Theory of orientation and stereoselection. In *Orientation and Stereoselection* (pp. 1-85). Berlin, Heidelberg: Springer Berlin Heidelberg.

González C, Schlegel HB. (1990). An improved algorithm for reaction path following. *Journal of Physical Chemistry* 94(14):5523–5527.

Hohenberg, P., & Kohn, W. (1964). Inhomogeneous electron gas. *Physical review*, *136*(3B), B864.

Jha M, Alam O, Naim MJ, Sharma V, Bhatia P, Sheikh AA, Siddiqui N. (2020). Recent advancement in the discovery and development of anti-epileptic biomolecules: An insight into structure activity relationship and docking. European Journal of Pharmaceutical Sciences 153:105494.

Karakurt T, Dincer M, Kahveci B, Usta A, Agar E, Sasmaz S. (2004). 3-(p-Chlorobenzyl)-4-(p-fluorobenzylideneamino)-4,5-dihydro-1H-1,2,4-triazol-5-one. Acta Crystallographica Section E-Crystallographic Communications 60(4):o654–o655.

Lee C, Yang W, Parr RG. (1988). Development of the Colle–Salvetti correlation-energy formula into a functional of the electron density. Physical Review B 37(2):785–789.

Martins MA, Frizzo CP, Moreira DN, Buriol L, Machado P. (2009). Solvent-free heterocyclic synthesis. Chemical Reviews 109(9):4140–4182.

Mennucci B. (2010). Continuum solvation models: What else can we learn from them? The Journal of Physical Chemistry Letters 1(10):1666–1674.

Parr RG, Pearson RG. (1983). Absolute hardness: companion parameter to absolute electronegativity. Journal of the American Chemical Society 105(26):7512–7516.

Parr RG, Szentpály LV, Liu S. (1999). Electrophilicity index. Journal of the American Chemical Society 121(9):1922–1924.

Pearson RG. (1987). Recent advances in the concept of hard and soft acids and bases. Journal of Chemical Education 64(7):561.

Raczynska ED, Cyranski MK, Gutowski M, Rak J, Gal JF, Maria PC, Duczmal K. (2003). Consequences of proton transfer in guanidine. Journal of Physical Organic Chemistry 16(2):91–106.

Reed AE, Curtiss LA, Weinhold F. (1988). Intermolecular interactions from a natural bond orbital, donor–acceptor viewpoint. Chemical Reviews 88(6):899–926.

Schlegel HB. (2003). Exploring potential energy surfaces for chemical reactions. *Journal of Computational Chemistry* 24(12):1514–1527.

Sobolewski AL, Domcke W. (2002). Hydrated hydronium: a cluster model of the solvated electron? Physical Chemistry Chemical Physics 4(1):4–10.

Xu Z, Zhao SJ, Liu Y. (2019). 1,2,3-Triazole-containing hybrids as potential anticancer agents: Current developments, action mechanisms and structure–activity relationships. European Journal of Medicinal Chemistry 183:111700.

Woodward RB, Hoffmann R. (1969). The conservation of orbital symmetry. Angewandte Chemie International Edition in English 8(11):781–853.

Zhan CG, Nichols JA, Dixon DA. (2003). Ionization potential, electron affinity, electronegativity, hardness, and electron excitation energy: molecular properties from density functional theory orbital energies. Journal of Physical Chemistry A 107(20):4184–4195.